# ADRC for Decentralized Load Frequency Control with Renewable Energy Generation

Sergio A. Dorado-Rojas*†
*Rensselaer Polytechnic Institute
Troy, NY USA
dorads@rpi.edu, sadorador@unal.edu.co

John Cortés-Romero†, Sergio Rivera†, Eduardo Mojica-Nava†
†Universidad Nacional de Colombia
Bogotá D.C., Colombia
{jacortesr, srriverar, eamojican}@unal.edu.co

***Abstract*—This document presents an application of Active Disturbance Rejection Control (ADRC) in a secondary frequency regulation problem with an active participation of renewable photovoltaic and wind generators. This problem is known as Load Frequency Control (LFC). The ADRC technique uses a reduced set of information of the model by grouping the effects of non-modeled dynamics, exogenous disturbances, and parameter uncertainties into a generalized equivalent disturbance, which in this case is estimated by an Extended-State Observer. This makes it possible to design a decentralized controller that achieves the bifold control objective of a secondary LFC strategy in each area. The proposed controller is able to regulate the frequency of each area and the tie-line power exchanges in presence of several load disturbances. The simulation scenarios validate the control proposal and show the flexibility and advantages of the application of ADRC-based control techniques as decentralized solutions to an LFC problem.**

***Index Terms*—Active Disturbance Rejection Control, Extended-State Observer, Load Frequency Control, Photovoltaic Generator, Wind Turbine Generator.**

## I. Introduction

Global warming and climate change have a direct impact on Electric Power Systems (EPSs), which are facing the complicated task of remaining in operational state while performing several structural transformations in order to allocate new clean generating units. As energy production is shifting to renewables, Wind Turbine Generators (WTGs) and Photovoltaic Generators (PVGs) emerge as the technologies with the fastest rate of growth in conventional EPSs.

On the other hand, the frequency in a traditional EPS is an excellent indicator of the balance between energy production and consumption (plus losses). Whenever the generation is adjusted to demand, the frequency remains constant. Nevertheless, system loads are constantly changing. Therefore, generator outputs must change automatically to be able to restore the frequency as fast as possible to its constant nominal value. For this purpose, an automatic control loop is designed. It is referred to as *Load Frequency Control* (LFC).

Due to the stochastic and variable nature of sunlight and wind, the power output of a PVG or a WTG changes steadily. Therefore, an LFC loop of an EPS with penetration of renewables must respond not only to loads but also to generation changes. This is not an issue in a large EPS with a significant amount of conventional generation, because the inertia of the synchronous units can overcome the variation introduced by PVGs and/or WTGs. Nevertheless, as the renewable energy share in an EPS increases, PVGs and WTGs must contribute actively to LFC in order to guarantee frequency stability and a correct system operation [1].

Renewable energy participation in LFC has been studied under the existence of storage systems (e.g., [2]). Nonetheless, some alternative control schemes have been proposed to enable renewable contribution within primary and secondary frequency control loops (e.g., [1], [3]). For this reason, we will deal with the problem of LFC in a power system with a high penetration of renewable resources. We propose a decentralized control strategy that allows renewable units – namely, WTGs and PVGs- to contribute actively to secondary frequency regulation.

To design the control strategy, the Active Disturbance Rejection Control (ADRC) paradigm is applied. The ADRC is a control design paradigm that represents an alternative between the model-based approaches and the empiric error-based alternatives [4]. The foregrounding idea behind ADRC is to employ less information from the model and to include a real-time estimation of a generalized disturbance into the control law that incorporates the effect of actual plant perturbations, model parameter uncertainties, and non-modeled dynamics.

An estimation of the generalized disturbance is usually obtained through an which is an Extended-State Observer (ESO) that, in addition to the model of the plant, comprises a model of the disturbance to be estimated. Depending on characteristics of the employed model, one can distinguish between several ADRC variants [5]. In particular, a Generalized Proportional Integral (GPI) observer strategy considers the disturbance signal to have the form of a smooth polynomial that can be approximated using a truncated Taylor series. This kind of techniques have been applied in a variety of problems such as the enhancement of LVRT capability in DFIG wind turbines [6]. Our proposed controller belongs to this category.

ADRC-based strategies have been applied in LFC problems without considering renewable energy generation (e.g., [7]). For instance, in [8], the ADRC proposal succeeds in incorporating a wind turbine into a primary frequency loop. Likewise, in [9], wind generators are accounted as a load disturbance, which is a common approach for considering renewable units in an LFC problem. Other similar control techniques that have been applied in EPSs with renewables are sliding-mode control

[10], and fractional-order control [11].

Our proposal consists of a decentralized linear ADRC secondary LFC strategy based upon an Extended-State Observer (ESO) for a multi-area power system with active renewable energy participation in frequency regulation. The ESO provides an estimation of an equivalent plant-input disturbance that is used to compensate the effects of load disturbances and to regulate the tie-line power flows without increasing the complexity of the control area model employed for the design.

The rest of the paper is organized as follows: Section II details the purposes of an LFC loop in an interconnected power system, and introduces the employed models of LFC components; Section III presents the fundamentals of the ADRC approach based upon an ESO; in Section IV, we describe of the case study and discuss the simulation results; and finally, Section V summarizes the conclusions of the work.

## II. Load Frequency Control (LFC)

### A. Foundations of LFC

The control action in an LFC loop is hierarchically classified as primary, secondary, tertiary, and emergency frequency control. The primary LFC, or droop control, takes advantage of the rotating inertia of synchronous generators by releasing the stored kinetic energy to compensate a small frequency deviation. This control action is performed locally in every generation unit, and aims to stabilize the frequency deviation at a permissible, constant value. This is typically a proportional control carried out by a governor thanks to a droop characteristic of each generator.

Similarly, secondary LFC takes place when an abnormal frequency deviation occurs. The purpose of this control loop is to restore the frequency $f$ to its nominal value $f_0$, or equivalently, to reduce the frequency deviation $\Delta f = f - f_0$ to zero. Tertiary and emergency levels correspond to discontinuous control actions, such as load or generation tripping, that prevent the system from entering a critical operation state.

The role of the secondary LFC loop is dual in interconnected power systems. In such scenarios, it is common practice to divide the system into control areas [1]. For instance, if a large power system is divided into three areas (Fig. 1), the LFC control loop has the additional task of ensuring that the power exchange between them remains within schedule. In other words, changes in the tie-line flows $\Delta P_{ij}$ must be equal to zero.

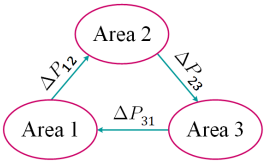


Fig. 1. Control areas within an EPS.

### B. Generalized Frequency Response Model

The interaction between the LFC components can be described by means of a generalized frequency response model (Fig. 2), which describes the $i$th control area within the system under consideration.

In this model, each control area is assumed to have $n_i$ generators. Moreover, it is common to assume that every generator engages in secondary frequency regulation thanks to a participation factor $\alpha_{n_i}$ so that $0 \leq \alpha_{n_i} \leq 1$ [1], [7]. Participation factors for each control area are determined by the market operator, and they satisfy $\sum_{i=1}^{n_i} \alpha_{n_i} = 1$. In this diagram, $\Delta P_{L,i}$ is the load disturbance and $\Delta P_{RES,i}$ is the change in renewable energy generation (considered as a negative load) that must be compensated by the LFC loop. $R_i$ is the $i$th unit droop characteristic. The frequency bias factor $B_i$ is obtained from the equivalent droop characteristic $R_{eq,i}$ by $B_i = D_i + 1/R_{eq}$, where $1/R_{eq} = \sum_{i=1}^{n_i} 1/R_i$, with $D_i$ being the load damping factor of the area.

The Area Control Error (ACE) is a quantity that synthesizes the twofold control objective of the secondary LFC. Assume that the $i$th control area exchanges active power with its neighboring control area $N_i$. Then, the ACE can be calculated from a linear combination of the frequency deviation and the tie-line flow deviations as

$$\mathrm{ACE}_i = B_i \Delta\omega_i + \sum_{j \in N_i} T_{ij} \frac{1}{s} \left( \Delta\omega_i - v_i \right). \tag{1}$$

The tie-line flows have been approximated by the synchronizing torque coefficients $T_{ij}$ and a signal $v_i$ known as area interface signal [1]. Note that if the signal $\mathrm{ACE}_i$ is reduced to zero, the tie-line flows and the frequency deviation are regulated.

It is worth mentioning that the generalized frequency response model has several series and parallel interconnections between blocks. Therefore, a transfer function analysis results more convenient. The transfer function from $\Delta P_{c,i}$ to $\Delta\omega_i$ is required for the controller design. It is written as $G_{A,i}(s)$ and can be computed as [7]

$$G_{A,i}(s) = \frac{\Delta\omega_i}{\Delta P_{c,i}} = \frac{G_{rm,i}(s) \sum_{j=1}^{n_i} \alpha_{ij} G_{GT,i}(s)}{1 + \sum_{j=1}^{n_i} \frac{\alpha_{ij} G_{GT,i}(s)}{R_j}}, \tag{2}$$

where $G_{rm,i}(s)$ are the rotating mass inertia dynamics of the $i$th area, $\alpha_{ij}$ is the participation factor of the $j$th generator, $G_{GT,i}(s)$ is the governor and turbine dynamics (or the corresponding reference-output power dynamics), and $R_j$ is the droop of the $j$th generation unit.

### C. Models for LFC Components

In this subsection, we introduce linear transfer function models for each LFC loop component. For the case of PVGs and WTGs, a conceptual explanation is given of how such renewable generators can participate in a secondary frequency control scheme.

*1) Photovoltaic Generator in LFC:* the fundamental building block of a Photovoltaic Generator (PVG) is a PV cell, which produces electricity from sunlight by virtue of the photoelectric effect. PV cells are connected in series to constitute a PV module. PV modules are arranged in series and parallel interconnections to form a larger generating unit known as PV array. Several PV arrays are organized in series and parallel fashions to construct a PVG.

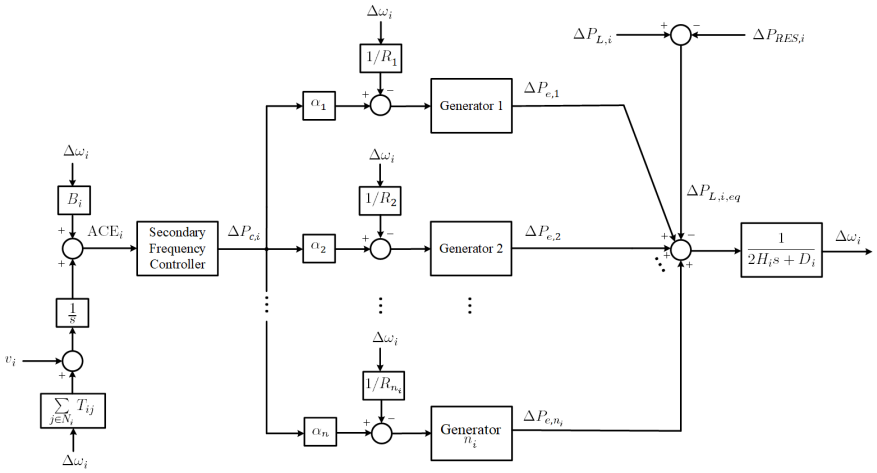


Fig. 2. Generalized frequency response scheme [1].

The output terminals of a PVG are connected to a DC-DC buck-boost converter that interfaces with a three-phase inverter that links the PVG to the grid. The buck-boost converter is responsible for controlling the power output of a PVG by regulating the terminal voltage. Usually, the terminal voltage control scheme aims to track the maximum power point voltage, a strategy known as Maximum Power Point Tracking (MPPT), to maximize the output power of the PVG. However, it is possible to operate the unit a set point different from the one dictated by the MPPT to keep a power reserve that enables the PV to provide frequency regulation capabilities.

A simplified linear transfer function model of a PVG for LFC is presented in [3]. With the parameter values for the buck-boost converter and the PV cell given in [12], the dynamics from power reference to PV power output are found to be strongly dominated by the following transfer function for a 1 MW unit:

$$G_{pv,\text{LFC}}(s) = \frac{\Delta p_{pv}}{\Delta p_{\text{ref}}} \approx 2.18\left(\frac{s+10}{s+21.76}\right). \tag{3}$$

*2) Photovoltaic Generator as a Negative Load:* normally, the effects of renewable energy generation in frequency dynamics are compensated by conventional generators [1]. From the control viewpoint, this approach consists in viewing a renewable source as a negative load disturbance to the control loop (e.g., [9]). A suitable model for incorporating this behavior into an LFC problem was introduced in [13] and is given by

$$G_{pv,\text{load}}(s) = \frac{\Delta P_{pv}}{\Delta G} = \frac{K_{pv}}{T_{pv}s+1}, \tag{4}$$

where $\Delta P_{pv}$ is the change in the generated electric power and $\Delta G$ is the variation in solar irradiance. In this model, $K_{pv} = 1$ and $T_{pv} = 1.8$ s.

*3) Wind Turbine Generator (WTG):* in practice, the most common variable speed wind turbine technology is the Doubly Fed Induction Generator (DFIG). A DFIG is operated using the Maximum Power Curve to maximize its power output in the existing wind conditions. Consequently –in a similar way to the case of PVGs- the main idea behind WTG frequency control participation is to reserve an amount of the available power so that the power reference of the control loop can be changed depending on the frequency deviation of the system. In this way, the generation unit will be capable of providing active power in order to balance the system frequency. Such a control scheme is detailed in [1].

A linear WTG model suitable for LFC studies was introduced in [14]. It has been successfully applied in LFC works such as [15]. This model consists of two transfer functions and is written as

$$G_w(s) = G_{wp}(s)\, G_{wl}(s)\, K_{PC}. \tag{5}$$

The first transfer function, $G_{wp}(s)$, models the variation in output power by a change on the pitch angle of the blades using a pitch actuator. It is given by

$$G_{wp}(s) = \left(\frac{K_{P1}(T_{P1}s+1)}{s+1}\right)\left(\frac{1}{T_{P2}s+1}\right), \tag{6}$$

where $K_{P1} = 1.25$ is the pitch actuator gain, and $T_{P1} = 6.0$ s and $T_{P2} = 0.041$ s are the time constants of the process. The second transfer function, $G_{wl}(s)$, is a first-order lag employed to match the phase/gain characteristics of the model to the experimental data. It is found as

$$G_{wl}(s) = \frac{K_{P2}}{s+1}, \tag{7}$$

where $K_{P2}$ is a constant. Finally, the parameter $K_{PC}$ is known as blade characteristic and has a constant value $K_{PC} = 0.80$ [14]. We take the droop of each WTG unit as $R_w = 0.024$.

*4) Hydraulic Generator:* under several assumptions, a lossless linear model of a hydraulic generator can be suitable for LFC studies. It consists of cascading the transfer function models of a governor and a turbine, as follows:

$$G_h(s) = \overbrace{\left(\frac{1}{1+T_Gs}\right)\left(\frac{1+T_Rs}{1+\left(\frac{R_T}{R_P}\right)T_Rs}\right)}^{\text{Governor}}\underbrace{\left(\frac{1-T_ws}{1+0.5T_ws}\right)}_{\text{Turbine}}. \tag{8}$$

In this model, the first transfer function describes the governor dynamics. The second is known as transient droop

compensation, and is required to compensate the effects of the non-minimum phase hydraulic turbine transfer function.

*5) Thermal Generator:* a thermal generator produces electricity after a boiling process, which is driven by materials such as coil, gas, and nuclear substances. Thermal generators use turbines that are commonly classified as reheat and non-reheat turbines. The reheating process makes reheat units more efficient that non-reheat ones. A transfer function model of the governor-turbine interconnection of a reheat unit is

$$G_T(s) = \overbrace{\left(\frac{1}{1+T_G s}\right)}^{\text{Governor}} \underbrace{\left(\frac{1+F_{HP}T_{RH}s}{(1+T_{CH}s)(1+T_{RH}s)}\right)}_{\text{Turbine}}, \tag{9}$$

where $T_G$ is the time constant of the governor, $F_{HP}$ is the fraction of the total turbine power generated in the high-pressure stage, $T_{RH}$ is the time constant of the reheating system, and $T_{CH}$ is the time constant of the steam boiling process.

*6) Rotating Mass Inertia:* the well-known swing equation describes the dynamics between active power and electric frequency in a rotating machine. Assume that the $i$th control area in an EPS has $n_i$ synchronous generators. Then, the rotating mass inertia dynamics can be described by the following transfer function:

$$G_{rm,i}(s) = \frac{1}{2H_i s + D_i}, \tag{10}$$

where $H_i$ is the aggregated inertia coefficient and $D_i$ is the load damping coefficient. A standard value for $D_i$ is $D_i = 2.0$. The aggregated inertia coefficient is computed from the inertia coefficient of every synchronous generator in the control area and its rated power (in MVA) as

$$H_i = \frac{\sum_{j=1}^{n_i} H_j S_j}{\sum_{j=1}^{n_i} S_j}. \tag{11}$$

## III. Control Design

Our proposal consists of a local ESO-based LFC controller that attempts to regulate the ACE and the frequency deviation within each control area. Since this control law does not directly depend on the frequency deviation of the neighboring areas, it is said to be decentralized. Moreover, we underline that tie-line power flows can be seen as an exogenous disturbance. Thus, their effects can be included within the equivalent input disturbance $\xi_i$ of each control area. Therefore, it is not necessary to compute the more complex transfer function from $\Delta P_{c,i}$ to $\text{ACE}_i$ and perform the design with the plant model given in Eq. (2). Likewise, this control design approach does not need to account the frequency bias factor in the plant model.

Consider a state-space realization of the $m_i$th transfer function in Eq. (2) given by

$$\begin{aligned} \dot{\mathbf{x}}_i &= \mathbf{A}_i \mathbf{x}_i + \mathbf{B}_i u_i \\ y_i &= \mathbf{C}_i \mathbf{x}_i, \end{aligned} \tag{12}$$

where $\mathbf{x}_i \in \mathbb{R}^{m_i \times 1}$, $\mathbf{A}_i \in \mathbb{R}^{m_i \times m_i}$, $\mathbf{B}_i \in \mathbb{R}^{m_i \times 1}$ and $\mathbf{C}_i \in \mathbb{R}^{1 \times m_i}$. Suppose there is a disturbance $\xi_i$ at the input of the plant. According to the ADRC paradigm, this input disturbance can represent not only an actual plant input perturbation, but also the effect of output-coupled disturbances, non-modeled dynamics, and parameter variations [4]. Therefore, it is called a generalized equivalent plant-input disturbance.

If we include the effect of $\xi_i$ into the dynamics of the system, the state-space description of the plant becomes

$$\begin{aligned} \dot{\mathbf{x}}_i &= \mathbf{A}_i \mathbf{x}_i + \mathbf{B}_i (u_i + \xi_i) \\ y_i &= \mathbf{C}_i \mathbf{x}_i. \end{aligned} \tag{13}$$

Now, let the generalized disturbance signal correspond to a smooth polynomial function that can be approximated by a $k$th order truncated Taylor series. In other words, we are assuming that the internal model of $\xi_i$ (i.e., the model of the LTI system that generates it) is of $k$th order. Let one of the state variables of the internal model, for instance $x_{\xi_i,1}$, to coincide with the disturbance $\xi_i$. Thus, $x_{\xi_i,1} = \xi_i$ and $x_{\xi_i,1}^{(k)} = \xi_i^{(k)} = 0$. The remaining $k-1$ state equations can be obtained by defining $\dot{x}_{\xi_i,j} = x_{\xi_i,j+1}$ for $j = 1, 2, \ldots, k-1$. Therefore, we have the following state-space model:

$$\begin{aligned} \dot{\mathbf{x}}_{\xi_i} &= \mathbf{A}_{\xi_i} \mathbf{x}_{\xi_i} + \mathbf{B}_{\xi_i} \xi_i^{(k-1)} \\ \xi_i &= \mathbf{C}_{\xi_i} \mathbf{x}_{\xi_i}, \end{aligned} \tag{14}$$

where $\xi_i^{(k-1)}$ is the $(k-1)$th time derivative of $\xi_i$, taken as the input of the model, and $k$ is the number of extended states. The value of $k$ can be selected by analyzing the shape of the disturbance signals (Fig. 4). The disturbance profiles show step, ramp and parabolic behaviors, which correspond to polynomial functions of maximum degree two. Thus, $k = 3$ results in an adequate number of extended states. The matrices $\mathbf{A}_{\xi_i}$, $\mathbf{B}_{\xi_i}$ and $\mathbf{C}_{\xi_i}$ are

$$\begin{aligned} (\mathbf{A}_{\xi_i})_{3\times 3} &= \begin{bmatrix} 0 & 1 & 0 \\ 0 & 0 & 1 \\ 0 & 0 & 0 \end{bmatrix} \\ (\mathbf{B}_{\xi_i})_{3\times 1} &= \begin{bmatrix} 0 \\ 0 \\ 1 \end{bmatrix} \\ (\mathbf{C}_{\xi_i})_{1\times 3} &= \begin{bmatrix} 1 & 0 & 0 \end{bmatrix} \end{aligned} \tag{15}$$

Considering the internal model of $\xi_i$, we can write the dynamics of the plant as

$$\begin{aligned} \dot{\mathbf{x}}_i &= \mathbf{A}_i \mathbf{x}_i + \mathbf{B}_i (u_i + \mathbf{C}_i \mathbf{x}_{\xi_i}) \\ y_i &= \mathbf{C}_i \mathbf{x}_i \end{aligned}. \tag{16}$$

At this point, we will include the dynamics of the plant and the internal model of $\xi_i$ into a single state-space representation, which is known as an extended system. The extended state is defined as $\bar{\mathbf{x}}_i \coloneqq \begin{bmatrix} \mathbf{x}_i^T & \mathbf{x}_{\xi_i}^T \end{bmatrix}^T$. Therefore, the dynamics of the extended system are given by

$$\begin{aligned} \dot{\bar{\mathbf{x}}}_i &= \overbrace{\left[\begin{array}{c|c} \mathbf{A}_i & \mathbf{B}_i \mathbf{C}_{\xi_i} \\ \hline \mathbf{0} & \mathbf{A}_{\xi_i} \end{array}\right]}^{\bar{\mathbf{A}}_i} \left[\begin{array}{c} \mathbf{x}_i \\ \hline \mathbf{x}_{\xi_i} \end{array}\right] + \overbrace{\begin{bmatrix} \mathbf{B}_i \\ \mathbf{0} \end{bmatrix}}^{\bar{\mathbf{B}}_i} u_i + \overbrace{\begin{bmatrix} \mathbf{0} \\ \mathbf{B}_{\xi_i} \end{bmatrix}}^{\bar{\mathbf{E}}_i} \xi_i^{(k-1)} \\ y_i &= \overbrace{\begin{bmatrix} \mathbf{C}_i & \mathbf{0} \end{bmatrix}}^{\bar{\mathbf{C}}_i} \left[\begin{array}{c} \mathbf{x}_i \\ \hline \mathbf{x}_{\xi_i} \end{array}\right] \end{aligned} \tag{17}$$

which is short-written as

$$\begin{aligned}\dot{\bar{\mathbf{x}}}_i &= \bar{\mathbf{A}}_i\bar{\mathbf{x}}_i + \bar{\mathbf{B}}_i u_i + \bar{\mathbf{E}}_i\xi_i^{(k-1)} \\ y_i &= \bar{\mathbf{C}}_i\bar{\mathbf{x}}_i \ .\end{aligned} \tag{18}$$

If we design a closed-loop observer for the extended system, we obtain an estimate of the extended state $\hat{\bar{\mathbf{x}}}_i$, from which we can recover an estimation of both the system state $\hat{\mathbf{x}}_i$ and the disturbance signal $\hat{\xi}_i$. This kind of observer is known as an Extended-State Observer (ESO).

Using the estimate provided by an ESO, we can cancel the equivalent disturbance of the plant in a feedback linearization-like control law. The proposed control law has the following form:

$$\Delta P_{c,i} = -\hat{\xi}_i - \mathbf{K}_i\hat{\mathbf{x}}_i \tag{19}$$

where $\mathbf{K}_i$ is the state feedback gain. This gain is selected by using the solution of a Linear Quadratic Regulator problem computed using the MATLAB function `lqr`.

## IV. Simulation Results

The IEEE-39 Bus New England System was selected as a baseline for the case study. This system was divided into three control areas and modified to add PVGs and WTGs in certain nodes of the system, as shown in Fig. 3.

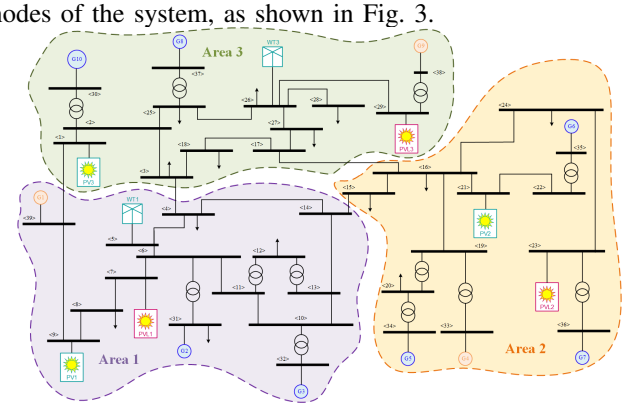


Fig. 3. Modified IEEE 39-Bus New England system with additional PVGs and WTGs. Orange generators correspond to reheat steam units, whereas blue ones are hydraulic generators. Renewable units participating in secondary LFC are drawn in turquoise. PVGs considered as negative load disturbances are colored in dark red.

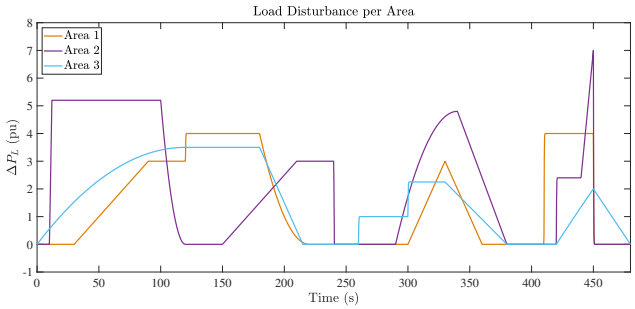


Fig. 4. Load disturbance $\Delta P_{L,i}$ for each control area.

In Areas 1 and 3, a PVG and a WTG participate simultaneously in the secondary frequency regulation; in Area 2, only a PVG is considered. Furthermore, all control areas have a PVG seen as a negative load, whose irradiance variation was assumed to be random. The disturbance load signals for each control area are shown below in Fig. 4. They are composed of step, triangular, and parabolic signals, which are commonly applied in LFC studies.

The parameters for the hydraulic and thermal generators were taken from [16]. The values of the synchronizing torque coefficients were assumed as $T_{12} = 2.5$, $T_{13} = 5.0$, and $T_{23} = 3.8$. The participation factors for each area were selected in such a way that the largest contribution for secondary LFC came from the thermal units, which normally provide spinning reserves to the system. The selected values were: $\alpha_{G1} = 0.500$, $\alpha_{G2} = 0.125$, $\alpha_{G3} = 0.125$, $\alpha_{WT1} = 0.125$, $\alpha_{PV1} = 0.125$ (Area 1); $\alpha_{G4} = 0.500$, $\alpha_{G5} = 0.100$, $\alpha_{G6} = 0.100$, $\alpha_{G7} = 0.100$, $\alpha_{PV2} = 0.200$ (Area 2); and $\alpha_{G8} = 0.125$, $\alpha_{G9} = 0.500$, $\alpha_{G10} = 0.125$, $\alpha_{WT3} = 0.125$, $\alpha_{PV3} = 0.125$ (Area 3).

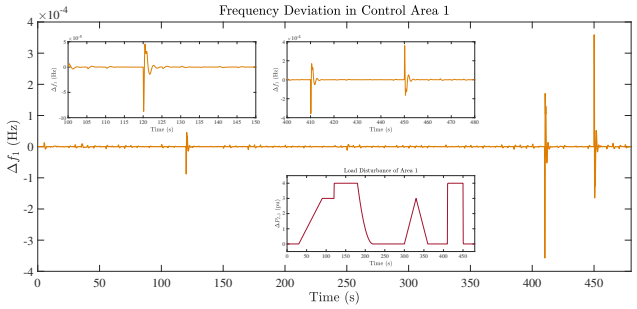


(a) Frequency deviation and load disturbance in Area 1.

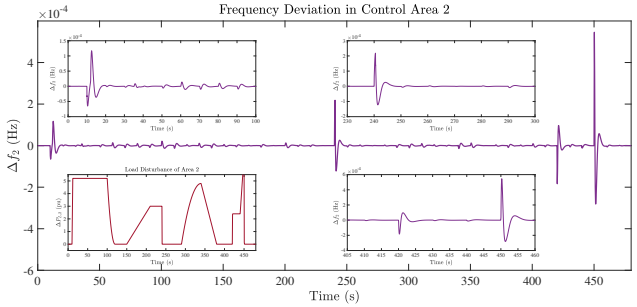


(b) Frequency deviation and load disturbance in Area 2.

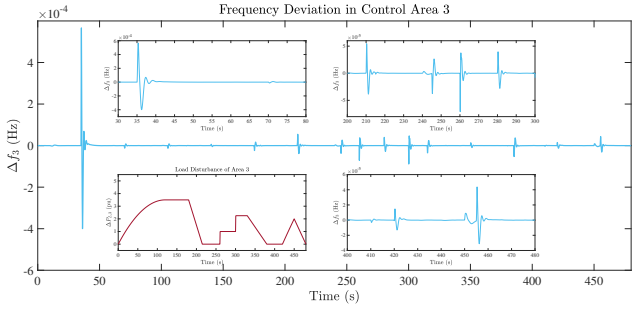


(c) Frequency deviation and load disturbance in Area 3.

Fig. 5. Frequency deviation and load disturbance for each control area.

As shown in Fig. 5, the ESO-based decentralized ADRC controller keeps the frequency deviation close to zero in all areas in spite of the load disturbances and the random variation of the PV generators considered as negative loads.

In fact, the frequency deviation drops to zero in steady-state after the transient vanishes. However, since the load distur-

bance signals change continuously, the frequency deviation is never identically to zero, but the observed variations have a small magnitude (less than 0.1 mHz).

The ESO-based ADRC controller was benchmarked against the control law $\Delta P_{c,i} = -\mathbf{K}_i \hat{\mathbf{x}}_i$ that does not employ the estimated generalized disturbance $\hat{\xi}_i$ for control purposes. The state feedback-based controller without disturbance rejection is not capable of regulating the frequency, as shown in Fig 6. One cause of this behavior is that the plant model used to design this state feedback was incomplete. For this controller to be effective, the employed model must contain the information of each control area from $\Delta P_{c,i}$ to $\text{ACE}_i$.

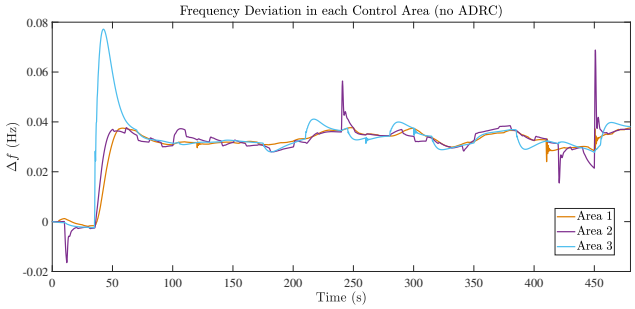


Fig. 6. Frequency deviation $\Delta f$ in each control area without ADRC.

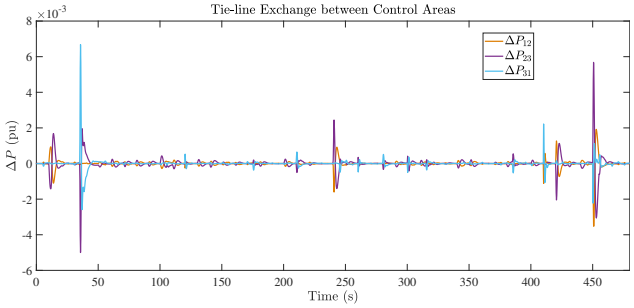


(a) Tie-line power exchange between control areas with ADRC.

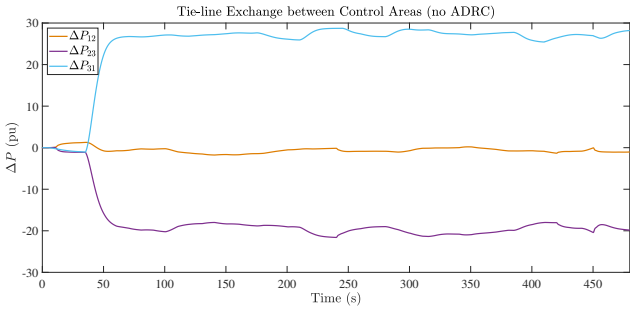


(b) Tie-line power exchange between control areas without ADRC.

Fig. 7. Tie-line power exchange between control areas.

Moreover, the decentralized ADRC strategy succeeds in regulating the tie-line power exchange (Fig. 7) between control areas, even when the tie-line exchange dynamics were not accounted into the model in Eq. (2). The control strategy without ADRC does not keep the tie-line power flow within scheduled values.

## V. Conclusions

This work has demonstrated the capabilities of a linear ADRC control strategy in a LFC multi-area problem. Renewable energy generators, such as PVGs and WTGs, are actively accounted into the secondary frequency regulation loop by means of linear models that describe a change in the set point of the corresponding power capture mechanism.

The application of the ADRC design paradigm made it possible to design a simple LQR control law without considering the more complex dynamics of the power exchange between control areas. The proposed ESO-based ADRC decentralized controller regulates the frequency and the tie-line exchange in the presence of constant load disturbances and random variations in power injections from PV generators thanks to a feedback linearization-like cancellation of a generalized equivalent plant input disturbance.

## References


[1] H. Bevrani, *Robust Power System Frequency Control*, 2nd ed. Springer, 2014.

[2] A. Zurfi and J. Zhang, "Exploitation of Battery Energy Storage in Load Frequency Control -A Literature Survey," *American Journal of Engineering and Applied Sciences*, vol. 9, no. 4, pp. 1173–1188, apr 2016.

[3] S. I. Nanou, A. G. Papakonstantinou, and S. A. Papathanassiou, "A generic model of two-stage grid-connected PV systems with primary frequency response and inertia emulation," *Electric Power Systems Research*, vol. 127, pp. 186–196, oct 2015.

[4] Zhiqiang Gao, "Active disturbance rejection control: a paradigm shift in feedback control system design," in *2006 American Control Conference*. IEEE, 2006, p. 7 pp.

[5] H. Sira-Ramírez, "From flatness, GPI observers, GPI control and flat filters to observer-based ADRC," *Control Theory and Technology*, vol. 16, no. 4, pp. 249–260, nov 2018.

[6] A. Beltran-Pulido, J. Cortes-Romero, and H. Coral-Enriquez, "Robust Active Disturbance Rejection Control for LVRT capability enhancement of DFIG-based wind turbines," *Control Engineering Practice*, vol. 77, pp. 174–189, aug 2018.

[7] C. Fu and W. Tan, "Decentralised load frequency control for power systems with communication delays via active disturbance rejection," *IET Generation, Transmission & Distribution*, nov 2017.

[8] Y. Tang, Y. Bai, C. Huang, and B. Du, "Linear active disturbance rejection-based load frequency control concerning high penetration of wind energy," *Energy Conversion and Management*, vol. 95, pp. 259–271, may 2015.

[9] C. Chen, K. Zhang, K. Yuan, and W. Wang, "Extended Partial States Observer Based Load Frequency Control Scheme Design For Multi-area Power System Considering Wind Energy Integration," *IFAC-PapersOnLine*, vol. 50, no. 1, pp. 4388–4393, jul 2017.

[10] K. Liao and Y. Xu, "A Robust Load Frequency Control Scheme for Power Systems Based on Second-Order Sliding Mode and Extended Disturbance Observer," *IEEE Transactions on Industrial Informatics*, vol. 14, no. 7, pp. 3076–3086, jul 2018.

[11] S. Saxena, "Load frequency control strategy via fractional-order controller and reduced-order modeling," *International Journal of Electrical Power & Energy Systems*, vol. 104, pp. 603–614, jan 2019.

[12] S. I. Nanou and S. A. Papathanassiou, "Modeling of a PV system with grid code compatibility," *Electric Power Systems Research*, vol. 116, pp. 301–310, nov 2014.

[13] Q. L. Guo and W. Tan, "Load Frequency Control of Hybrid Power Systems via Active Disturbance Rejection Control (ADRC)," *Applied Mechanics and Materials*, vol. 325-326, pp. 1145–1151, jun 2013.

[14] D. Das, S. Aditya, and D. Kothari, "Dynamics of diesel and wind turbine generators on an isolated power system," *International Journal of Electrical Power & Energy Systems*, vol. 21, no. 3, pp. 183–189, mar 1999.

[15] S. Ganguly, C. K. Shiva, and V. Mukherjee, "Frequency stabilization of isolated and grid connected hybrid power system models," *Journal of Energy Storage*, vol. 19, pp. 145–159, oct 2018.

[16] P. Demetriou, M. Asprou, J. Quiros-Tortos, and E. Kyriakides, "Dynamic IEEE Test Systems for Transient Analysis," *IEEE Systems Journal*, vol. 11, no. 4, pp. 1–10, 2015.